

A semi-active mass damping system for low- and mid-rise buildings

Pei-Yang Lin¹, Tzu-Kang Lin² and Jenn-Shin Hwang^{*3}

¹*National Center for Research on Earthquake Engineering, Taipei, Taiwan*

²*Department of Civil Engineering, National Chiao Tung University, Hsin-Chu, Taiwan*

³*Department of Construction Engineering, National Taiwan University of Science and Technology, Taipei, Taiwan*

(Received January 27, 2011, Revised February 1, 2012, Accepted February 22, 2012)

Abstract. A semi-active mass damping (SMD) system with magnetorheological (MR) dampers focusing on low- and mid-rise buildings is proposed in this paper. The main purpose of this study is to integrate the reliable characteristics of the traditional tuned mass damper (TMD) and the superior performance of the active mass damper (AMD) to the new system. In addition, the commonly seen solution of deploying dense seismic dampers throughout the structure nowadays to protect the main structure is also expected to switch to the developed SMD system on the roof with a similar reduction performance. In order to demonstrate this concept, a full-size three-story steel building representing a typical mid-rise building was used as the benchmark structure to verify its performance in real life. A numerical model with the interpolation technique integrated was first established to accurately predict the behavior of the MR dampers. The success of the method was proven through a performance test of the designated MR damper used in this research. With the support of the MR damper model, a specific control algorithm using a continuous-optimal control concept was then developed to protect the main structure while the response of the semi-active mass damper is discarded. The theoretical analysis and the experimental verification from a shaking table test both demonstrated the superior mitigation ability of the method. The proposed SMD system has been demonstrated to be readily implemented in practice.

Keywords: tuned mass damper; hybrid control; MR damper.

1. Introduction

The tuned mass damper (TMD) was first studied early in the 20th century. By adding an extra vibrating system to the primary vibrating system complete with proper stiffness and damping, the response of the main structure could be decreased significantly during external excitation such as by wind loading or from an earthquake. The early application of TMDs was an attempt to reduce the rolling motion of ships (Frahm 1911). After further development, the TMD was used to control the structural response in different fields (Ormondroyd and Den Hartog 1928, Brock 1946, Den Hartog 1947). The original design concept of the TMD was to figure out the optimal value of the frequency and damping ratio under white noise excitation. The performance of structures equipped

*Corresponding author, Professor, E-mail: JSH@mail.ntust.edu.tw

with a TMD under vibration beyond this basic assumption was questionable. To solve this difficulty, various theories were developed (Rudinger 2007, Bakre and Jangid 2007, Zuo and Nayfeh 2005).

Due to the passive dissipation characteristics of the dampers and the difficulty of implementing a high mass ratio in practice, a pure TMD can only offer limited reduction of a structural response. Moreover, the initial rest condition of the TMD makes it impossible to offer a rapid suppression during the first stage of earthquake excitation, which often is the period that causes the most severe property damage. For that reason, TMD systems are used mainly to mitigate wind turbulence. Two significant practical applications of TMDs are the John Hancock Tower in Boston, MA, 1975, and the Citicorp Center in New York, NY, 1976. Both were installed to mitigate the possible response from wind excitation.

To improve the performance of reducing the structural reaction, the active mass damper (AMD) was proposed. Rather than only absorbing the energy from the building, the AMD can supply or dissipate energy to the main structure by applying the proper force from the active device. For example, a control algorithm was developed for the AMD to successfully alleviate the response of two slender, wind-loaded buildings 200 m and 400 m tall respectively, to a level acceptable for human comfort (Mackriell *et al.* 1997). The results from other research also have proven that AMDs can effectively ameliorate the reaction of tall buildings under either seismic or wind loading in a numerical simulation (Qu *et al.* 2001, Chang and Yang 1995, Loh and Chern 1994). For the last two decades, many active mass dampers have been installed to actual civil engineering structures, mostly located in Japan, for either research and development activities or practical applications, and their effectiveness has already been verified through observation records (Sakamoto *et al.* 1996, Nishitani and Inoue 2001, Yamamoto *et al.* 2001). However, the costly and complex control system combined with some reliability and maintenance issues are still the main reasons why AMDs are not implemented widely.

Over the past decade, the concept of semi-active tuned mass dampers (STMD) has been widely discussed. The idea of the STMD is to try and combine the advantages from both the TMD and the AMD, thereby optimizing the frequency and the damping ratio in an adaptive and reliable manner. On this premise, a large amount of research was conducted to offer protection for civil structures (Ricciardelli *et al.* 2000, Yang *et al.* 2002, Setareh 2001). The research by T. Pinkaew proved that the utilization of STMDs could be equivalent to increasing the TMD's mass in the structure, which was the main constraint in designing a TMD system (Pinkaew and Fujino 2001). Even though all the numerical studies have shown satisfactory results for the STMD, one basic condition has always been assumed in the research: the stiffness and the damping of the STMD must be varied in a reasonably short period of time. This has proven to be the bottleneck confining the practicability of the STMD.

The discovery of magnetorheological (MR) fluid can be traced back to the late 1940s (Rabinow 1948). MR fluid has the unique characteristic of being readily controlled using a low voltage (e.g. 0-1.2~2.4 V) and a small current-driven power supply output (0-1~2 amps). It also has shown to have great potential to transform a traditional passive damper into a semi-active control device. In the past decade a lot of research has been carried out, and the MR damper technology has matured. For example, Gregory *et al.* (2000) successfully utilized MR bracing systems to control civil structures by optimizing the location of the MR dampers (Gregory and Wereley 2000). Both theoretical analysis and experimental verification were executed using a steel frame structure on a shaking table to evaluate the practical performance of MR dampers (Renzi and Serino 2004). Recently, a toggle brace-MR damper system was proposed by Lee *et al.* (2007) to enhance the

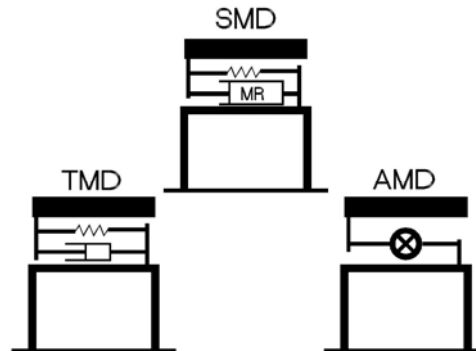


Fig. 1 Concept of the SMD with MR damper and RPS

performance of MR dampers (Lee *et al.* 2007).

A series of research including the investigation and simulation of the MR damper, as well as applying specific MR dampers to control an isolated structure were conducted by the authors. Kim *et al.* (2006) proposed a neuro-fuzzy model to describe the behavior of a hybrid system with friction pendulum system (FPS) bearings and an MR damper. Different control algorithms were then compared to offer strong protection to the main structure (Shook *et al.* 2007). At the same time the possibility of utilizing resettable semi-active stiffness dampers was investigated (Yang *et al.* 2007). Although the results showed that the utilization of MR dampers can provide a vastly superior next-generation control system, the MR dampers were mainly considered as bracing-type equipment and may not be feasible for practical structures when a large amount of MR damping is required.

As the stiffness and the damping of MR damper can be easily manipulated, it becomes an ideal candidate to implement the above-mentioned STMD concept. Meanwhile, for the swift mechanical reaction characteristic of MR damper, the STMD concept can be reached by further simplifying it to semi-active mass damping system (SMD) by utilizing the small initial stiffness and the large stroke characteristics, where the complicated tuning process can be neglected without losing any efficiency. In this paper a SMD utilizing MR dampers for low- and mid-rise buildings is proposed. The remainder of this paper is organized as follows. First, the main concept of the proposed system is described. Next, in order to precisely evaluate the behavior of the MR damper used in the research and to guarantee its application, we compared the performance test result of a specific MR damper with the numerical model developed. Then a numerical analysis and experimental verification are carried out to demonstrate the performance of the proposed SMD system. Finally a summary is given and conclusions are drawn.

2. Concept of the proposed system

The main objective of this research is to integrate the reliable characteristic of the traditional TMD and the superior performance of the AMD into the proposed system. The traditional TMD, shown in the bottom-left corner of Fig. 1, is commonly comprised of three parts: the mass block, the cable to supply the required tuned stiffness and the passive damper for the tuned damping. Although reliable control efficiency has been proven in the literature, two major difficulties remain:

the practical implementation of a high mass ratio and the huge space needed for the pendulum cable. These problems constrain the development of the TMD to high-rise buildings under wind excitation.

On the other hand, the AMD system shown in the bottom-right corner utilizes hydraulic actuators to actively control the mass block on top of the structure, providing a satisfactory performance. However, it is the inevitable robustness problem that determines the final fate of the AMD.

In this study, the idea of applying the combination of the roller pendulum system (RPS) and the MR damper as a novel SMD system on the top of a low- or mid-rise structure in order to obtain the advantages from both the TMD and the AMD is proposed. Unlike the inevitable small mass ratio constraint in high-rise buildings, the mass ratio of the proposed system is slightly increased by utilizing the possible facilities on the roof to enhance the reduction performance on structural response. The mass block is first isolated by the RPS for a specific period. Because of the frictionless and spaceless characteristic of the RPS system, the response of the main structure can be mitigated easily by manipulating the MR damper using a proper control algorithm. Moreover, the performance of the system can be guaranteed by the hybrid trait of the MR damper. The SMD concept can be easily realized utilizing the air conditioners or water tanks used in a building in real life with proper designed moveable pipe lines.

A four degree-of-freedom (DOF) model is used to express a three-story benchmark structure representing a typical mid-rise building with RPS and MR damper in this research. As shown in Fig. 2, only the longitudinal movement is considered with X_1 , X_2 and X_3 being the displacement of the main structure, and X_4 the response of the SMD on the roof. The first three fundamental frequencies of the main structure are set to 1.085, 3.277 and 5.165 Hz, and the mass on the first and second floor is 6 t (m_1 , m_2). The total mass of m_3 and m_4 is also set to 6 t where m_4 is the tunable mass block of the control system. The stiffness and period of the RPS used in this study are 1.049 kg/mm and 2.77 s, respectively. The response vector of the structure in the later derivation will follow the form of $[X_4 \ X_3 \ X_2 \ X_1]^T$.

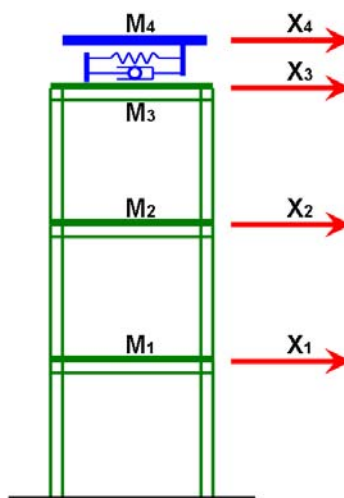


Fig. 2 Numerical model of the three-story structure with MR damper

Table 1 Specification of the MR damper

Specification		
	Type	MR2005
	Stroke	300 mm
	Force capacity	7 kN
Cylinder	Length	400 mm
	Outside diameter	100 mm
	Inside diameter	84.5 mm
Piston length	Length	800 mm
	Rod diameter	35 mm
	Head length	100 mm
Coil	Number of loops	200 loops
	Size	24 gauge

3. The proposed SMD system

The primary concept of the proposed SMD is to suppress the response of the main structure by sacrificing as much as possible the reaction of the mass added on top of the building. To achieve this goal, the stroke of the MR damper used becomes the most critical point in the system. A designated MR damper manufactured by the National Center for Research on Earthquake Engineering (NCREE) is used in this research. The basic property of the MR damper is shown in Table 1 where the maximum stroke is 300 mm.

The robust numerical model of the MR damper for describing its hysteresis behavior under arbitrary excitation is essential for developing the SMD system. Unlike the previous neuro-fuzzy model proposed by the authors (Kim *et al.* 2006), a novel approach based on the Bouc-Wen model is proposed in this study for both the theoretical and the experimental stages. According to the previous studies by Spencer *et al.* 1997 (Spencer *et al.* 1997), the Bouc-Wen model is suitable to describe the nonlinear behavior of the MR damper. To simplify the mathematic model, a modified form as shown in Eqs. (1) and (2) is used. Four parameters (C , α , β and γ) are used to express the performance of the MR damper under a fixed command voltage.

$$F_{MR}(t) = C * \dot{x}(t) + z(t) \quad (1)$$

$$\dot{z}(t) = \alpha * \dot{x}(t) + \beta |\dot{x}(t)| |z(t)| + \gamma \dot{x}(t) |z(t)|^2 \quad (2)$$

where F_{MR} represents the force, and $\dot{x}(t)$ represents the velocity of the MR damper.

Generally the nonlinear curve fitting method is used to find the unique relationship between the model parameters and the command voltages of a specific MR damper. However, the time required as well as the complex coefficients make this method impractical. This study simplified the relationship between the model parameters and the command voltage using a new technique of

interpolation. The performance test data of the MR damper with random displacement and seven constant voltage levels (0, 0.2, 0.4, 0.6, 0.8, 1 and 1.2 V) are used to identify the individual model parameters (C_i , α_i , β_i and γ_i , $i = 1 \dots 7$) for each constant command voltage level first. These parameters can be identified using Matlab/Optimization toolbox (MATLAB 1992). The identified model parameters of the seven constant voltage levels are shown in Table 2. The theoretical force of the MR damper with command voltage different from these seven levels can then be obtained by interpolating the model parameters from the two adjacent levels it locates.

Table 2 Identified model parameters of MR damper (Unit: kN-m-s)

Voltage (Volt)	C	α	β	γ
0	12.955	4628.659	-742.499	-187.583
0.2	16.729	5314.937	-690.171	422.641
0.4	20.887	8175.300	-201.144	108.644
0.6	24.048	10384.40	-139.423	65.465
0.8	27.756	6386.549	-107.805	68.691
1.0	25.319	8469.352	-99.669	57.789
1.2	26.274	9345.521	-87.724	46.546

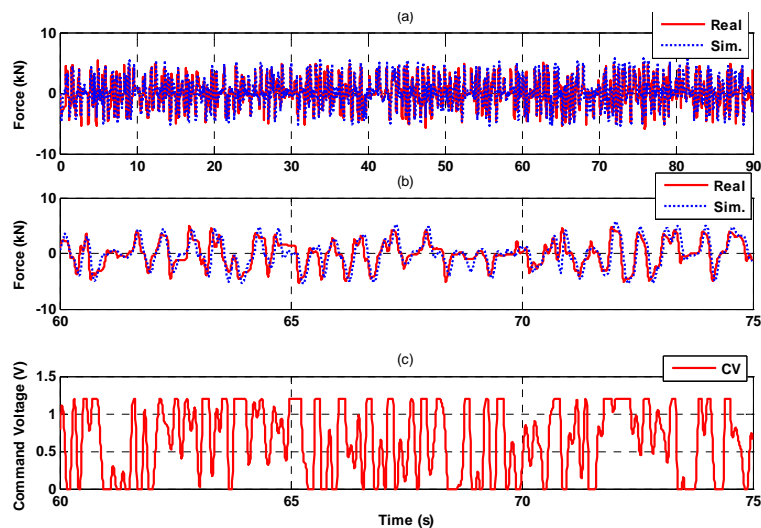


Fig. 3 Comparison of the real and the simulated MR damper force in the performance test (random displacement and random voltage): (a) the whole history, (b) the time history 60~75 sec and (c) command voltage to the MR damper

The numerical model of the MR damper established was verified through a performance test of the MR damper at NCREE. A banded white noise (0-5 Hz) was used as the velocity and voltage of the MR damper. 90 seconds of damping force were recorded, and the result is shown in Fig. 3 where subplot (a) shows the time history of the damping force, subplot (b) focuses on the period between 60 to 75 seconds and subplot (c) indicates the given command voltage. The numerical simulation, shown in red color substantially matches the measured response in blue color and the peak values and phases of the damping force can be expressed precisely by the proposed method. This result strongly supports that the proposed model can be applied in the present study.

The simulated and achieved hysteresis loops of the MR damper are shown in Fig. 4. The comparison once again proves the feasibility of applying the model for predicting the behavior of the MR damper. In addition, the performance test result also proves the superior energy dissipation ability of the MR damper.

To offer a strong protection to the structure, a special control algorithm and a continuous-optimal control concept is proposed. In this study, the traditional LQR method, the most common active control algorithm, is used as the basis to calculate the optimal control

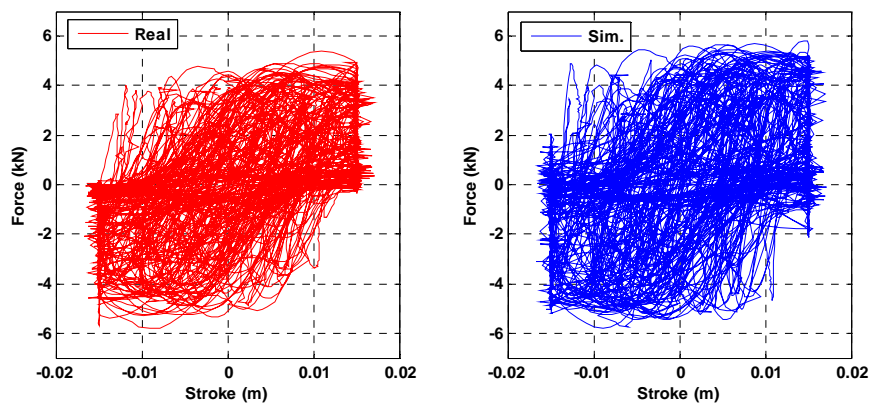


Fig. 4 Comparison of the real and the simulated hysteresis loop of the MR damper (random displacement and random voltage)

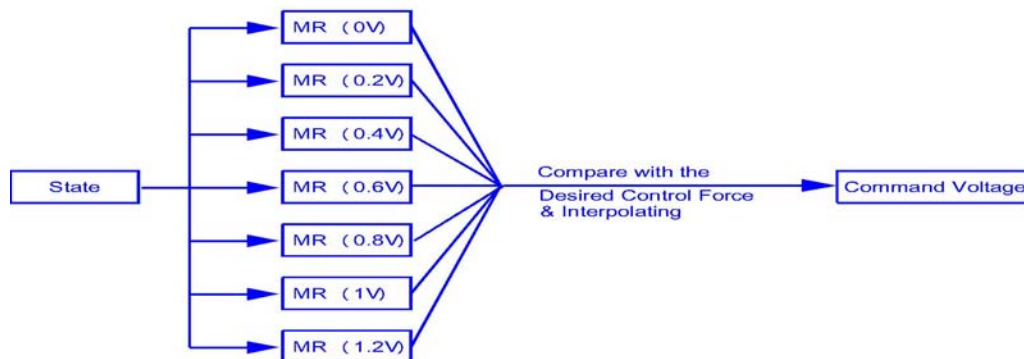


Fig. 5 Flow chart of the semi-active control strategy

force with designated control objectives to make the SMD system both simpler and more flexible. At the same time, while the damper force of the MR damper can be successfully described by utilizing highly nonlinear numerical model with the input of structural response and command voltage; however, Due to the highly nonlinear terms contained in the formula derived, calculating the proper command voltage corresponding to the designated damping force by reversing the numerical model with the structural response and the damper force presents a big challenge. Unlike the previous developed neural-network-based MR damper model facing the time-consuming extrapolation problems (Renzi and Serino 2004), the continuously-optimal control concept utilizing the MR damper model established in the previous section is proposed to transfer the desired control voltage from the optimal active control force obtained. Meanwhile, rather than interpolating the model parameters as in the previous section, the command voltage to the MR damper with the control force determined is obtained by directly interpolating the control force from the two adjacent levels of the seven models with different constant voltages it locates. By the new proposed continuous-optimal control concept, the command voltage to the MR damper can be improved from the clipped optimal control where the command voltage can only be the maximum or minimum value to continuous signal; therefore, a better and smoother control effect can be achieved. The flowchart of the continuous-optimal control concept is shown in Fig. 5.

The procedure for deriving the optimal control gain of the LQG method used in this research is illustrated in the next few paragraphs as follows:

For a structure, the equation of motion can be written in the state-space form as

$$\dot{X}(t) = A X(t) + B U(t) \quad (3)$$

Where $X(t)$ represents the state-space response of the structure (relative displacement and velocity); A is the system matrix and B is the excitation matrix.

As shown above, the displacement, velocity and acceleration of the structure can be easily obtained by using Eq. (3). However, if a specific response of the structure is desired, then Eq. (3) can be written as

$$Y(t) = C X(t) + D U(t) \quad (4)$$

where C and D are defined as the output matrices of the system.

Considering the output of Eq. (4), the performance index of the regular LQR control method can then be redefined as

$$J = \int_{t=0}^{\infty} \{Y^T(t) Q Y(t) + U^T(t) R U(t)\} dt \quad (5)$$

where Q is the response weighting matrix and R is the control force weighting matrix.

With the performance index defined in Eq. (6), the Ricatti equation shown in Eq. (5) can be used to solve the optimal control gain

$$C^T Q C + A^T P + P A - (P B + C^T Q D) (D^T Q D + R)^{-1} (B^T P + D^T Q C) = 0 \quad (6)$$

where P is a constant matrix.

The optimal control gain G can then finally be expressed as the following equation

$$G = -(D^T QD + R)^{-1} (B^T P + D^T QC) \quad (7)$$

In this study, the relative displacement, velocity and absolute acceleration of the 4 DOF system are used as the specific response of the structure listed in Eq. (8).

$$Y = [x, \dot{x}, \ddot{x}]^T \quad (8)$$

A designated response weighting matrix QQ is also appointed to implement the concept of mitigating the main structure response by sacrificing the reaction of the mass block on the roof.

$$Q = \begin{bmatrix} 10^{Q_{D1}} * QQ & 0 & 0 \\ 0 & 10^{Q_{V1}} * QQ & 0 \\ 0 & 0 & 10^{Q_{A1}} * QQ \end{bmatrix} \quad (9)$$

$$\text{Where } QQ = \begin{bmatrix} 1 & 0 & 0 & 0 \\ 0 & 1 & 0 & 0 \\ 0 & 0 & 1 & 0 \\ 0 & 0 & 0 & 0 \end{bmatrix}.$$

Moreover, the exponential form is used to express the control force weighting matrix R .

$$R = 10^{-R1} \quad (10)$$

The weighting parameter used to calculate the optimal control gain of the LQR method is listed in Eq. (11). The main objective of this set of weighting parameters is to reduce the displacement response of the main structure. At the same time, the floor acceleration and velocity responses are considered as well.

$$[Q_{D1} \quad Q_{V1} \quad Q_{A1} \quad R_1] = [6.2 \quad 3 \quad 5 \quad 9] \quad (11)$$

According to the desired control force, the command voltage is yielded by the interpolation between the best two voltage levels as shown in Eq. (12).

$$V = V_j * \frac{F_{desired} - F_{MR_{V_i}}}{F_{MR_{V_j}} - F_{MR_{V_i}}} + V_i * \frac{F_{MR_{V_i}} - F_{desired}}{F_{MR_{V_j}} - F_{MR_{V_i}}} \quad (12)$$

where V is the command voltage; V_i and V_j are the two closest voltages; $F_{MR_{V_i}}$ and $F_{MR_{V_j}}$ are the corresponding force of V_i and V_j ; and $F_{MR_{desired}}$ is the force calculated by the specific LQR method.

4. Theoretical evaluation of the SMD system

The theoretical performance of the developed SMD system is first verified by the 1940 El Centro earthquake (NS direction), which represents a typical earthquake. To demonstrate the capability of the proposed damping system, a full comparison is made, where the stroke and the

Table 3 Theoretical result of the El Centro earthquake with different PGA values

Control case		Added mass (kg)	Mass ratio	D_1 (m)	D_2 (m)	D_3 (m)	A_1 (m/s ²)	A_2 (m/s ²)	A_3 (m/s ²)	
ELC-100	UC			0.017	0.033	0.042	2.062	2.269	2.631	
	TMD	500	2.8%	0.015	0.028	0.036	1.950	1.899	2.025	
		1000	5.6%	0.018	0.035	0.044	1.931	1.842	2.203	
		1500	8.3%	0.016	0.030	0.038	1.918	1.811	1.995	
		2000	11.1%	0.015	0.029	0.038	1.905	1.782	2.158	
	AMD	500	2.8%	0.016	0.031	0.038	1.066	1.865	2.189	
		1000	5.6%	0.014	0.026	0.032	1.237	1.650	1.938	
		1500	8.3%	0.011	0.021	0.026	1.063	1.469	1.595	
		2000	11.1%	0.009	0.017	0.021	1.057	1.154	1.642	
	SMD	500	2.8%	0.017	0.032	0.040	1.622	1.827	2.188	
		1000	5.6%	0.015	0.029	0.036	1.532	1.886	2.343	
		1500	8.3%	0.013	0.024	0.030	1.481	1.786	2.496	
		2000	11.1%	0.011	0.020	0.025	1.456	1.592	1.841	
	ELC-200	UC			0.041	0.075	0.092	4.631	5.355	5.704
		TMD	500	2.8%	0.034	0.067	0.086	4.242	4.286	5.124
			1000	5.6%	0.038	0.071	0.090	4.188	4.126	4.746
1500			8.3%	0.035	0.063	0.077	4.159	4.049	4.519	
2000			11.1%	0.029	0.059	0.076	4.102	3.929	4.779	
AMD		500	2.8%	0.032	0.062	0.076	2.131	3.730	4.377	
		1000	5.6%	0.028	0.053	0.064	2.473	3.299	3.877	
		1500	8.3%	0.022	0.043	0.053	2.126	2.939	3.189	
		2000	11.1%	0.019	0.035	0.042	2.114	2.308	3.287	
SMD		500	2.8%	0.037	0.068	0.082	3.815	4.191	4.682	
		1000	5.6%	0.030	0.054	0.066	3.709	3.752	3.937	
		1500	8.3%	0.027	0.043	0.054	3.885	3.462	3.897	
		2000	11.1%	0.023	0.036	0.044	3.373	2.647	3.946	
ELC-300		UC			0.068	0.127	0.157	7.097	9.017	9.947
		TMD	500	2.8%	0.049	0.097	0.126	6.262	6.443	7.181
			1000	5.6%	0.061	0.119	0.152	6.181	6.211	7.880
	1500		8.3%	0.052	0.097	0.129	6.092	5.965	7.106	
	2000		11.1%	0.050	0.100	0.132	6.009	5.733	7.314	
	AMD	500	2.8%	0.048	0.093	0.113	3.197	5.595	6.566	
		1000	5.6%	0.042	0.079	0.097	3.710	4.948	5.816	
		1500	8.3%	0.033	0.064	0.079	3.189	4.408	4.783	
		2000	11.1%	0.028	0.052	0.064	3.172	3.463	4.932	
	SMD	500	2.8%	0.061	0.113	0.134	5.460	6.923	7.528	
		1000	5.6%	0.044	0.080	0.096	5.693	5.722	6.104	
		1500	8.3%	0.034	0.059	0.074	4.712	4.115	5.764	
		2000	11.1%	0.029	0.054	0.068	3.799	3.517	5.852	

reaction of the MR damper are not restricted. Four different cases including the uncontrolled mode (UC), tuned mass damper mode (TMD/combination of the RPS and MR damper in passive mode), active tuned mass damper mode (AMD) and the semi-active mass damper mode (SMD) are evaluated under peak ground acceleration (PGA) of 100 gal, 200 gal and 300 gal respectively. The traditional LQG control algorithm is utilized to control the AMD in this study. The peak value of the relative displacements (D_1 , D_2 and D_3) and the absolute accelerations (A_1 , A_2 and A_3) of the basic structure are listed in Tables 3. As the main control objectives of the SMD system are low- and mid-rise buildings, the mass ratio on the roof can be reasonably increased from the strict restriction used in high-rise buildings, which is commonly set to 1-2%. Four different mass ratios of 2.8%, 5.6%, 8.3% and 11.1% shown in the tables are fully simulated to evaluate the performance of the system where the added mass is set as 500, 1000, 1500 and 2000 kg compared to the structure mass of 18000 kg, respectively. The best performance under the same mass ratio is marked in boldface.

In the case of the 500 kg added mass under the El Centro earthquake with a PGA of 100 gal, obviously the structural response can be alleviated most by the TMD from 263.1 gal to 202.5 gal, or a 23.03% reduction while the SMD provides a 16.8% to 218.8 gal. The roof displacement is also ameliorated most by the TMD from 4.2 cm to 3.6 cm, or a reduction of 14.29% while the SMD provided only a reduction from 4.2 cm to 4.0 cm. The expected advantage of the SMD and AMD could not be realized under a low mass ratio.

However, when increasing the mass block to 1000, 1500 and 2000 kg, the semi-active and active system start to control the response of the structure while the displacement response is slightly exaggerated by the TMD due to the non-optimal mass ratio for the TMD concept. For example, with a mass ratio of 8.3%, a 1500kg mass block, the roof displacement is improved from 4.2 cm to 2.6 cm for the AMD system, and similar result can be reached by the proposed SMD to 3.6 cm. The absolute acceleration of the second floor is reduced from 226.9 gal to 178.6 gal, or a reduction of 21.28% in the SMD system and to 146.9 gal for the AMD. The result has shown that the structural response can be managed more effectively by the proposed SMD system than by the TMD system when the mass ratio is increased correctly. For the rapid controllability characteristic, structural response can be suppressed most in the AMD cases.

To clearly compare the performance of the SMD system under different mass ratios and PGA levels, Table 3 is converted into Figs. 6 and 7, and the important trends can be better observed. As expected, a better performance can be obtained by increasing the mass on the top of the structure in all systems. The response drops more sharply as the mass of the block is increased. Similar performance to the AMD can be achieved by the SMD. However, constrained by the specification of the MR damper using used in the experimental verification, as listed in Table 1, only the satisfactory improvement from the TMD to SMD can be investigated when facing larger PGA values, which are defined as major earthquakes. With the optimized design of the MR damper for the structure, the proposed SMD system can adaptively adjust its control gain according to the structural response and work appropriately for all levels of earthquakes.

The stroke, velocity and control force of both AMD and SMD are shown in Fig. 8. For the case of the 500 kg added mass under the El Centro earthquake with a PGA of 300 gal. The stroke of the AMD is almost twice of that of the SMD, and only similar performance is reached. This large stroke may cause a serious problem in designing a proper AMD system. When the mass block is increased to 2000 kg, the control force required by the AMD is also almost twice of the SMD. For example, in the case of El Centro earthquake with a PGA of 300 gal, the maximum control force of the SMD is confined to 500kg while approximately 850 kg is demanded by the AMD. In short,

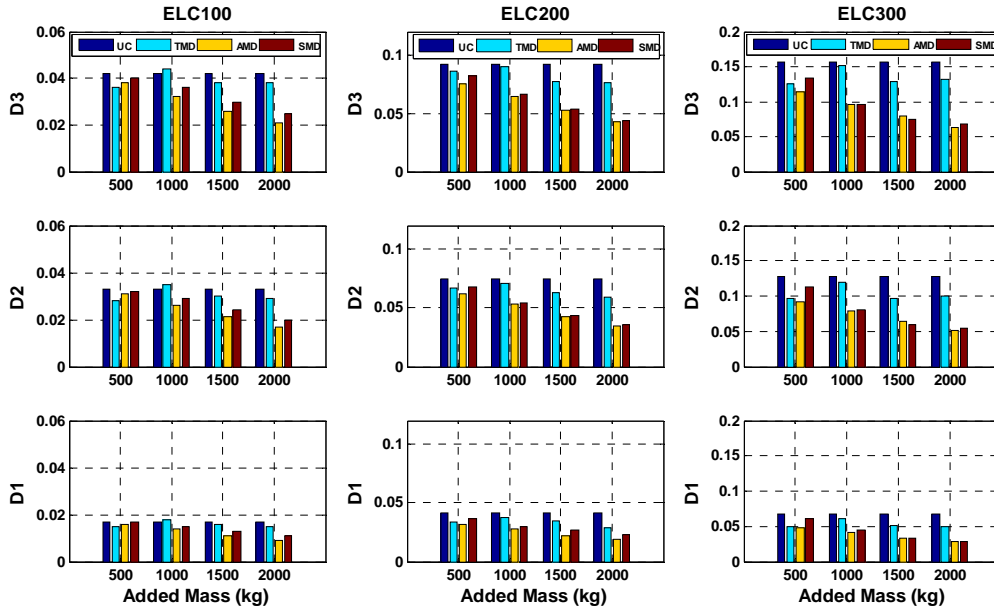


Fig. 6 Comparison of the maximum displacement responses of uncontrolled structure, structure with passive TMD and semi-active SMD with different added mass under El Centro earthquakes (normalized to 100, 200 and 300 gals)

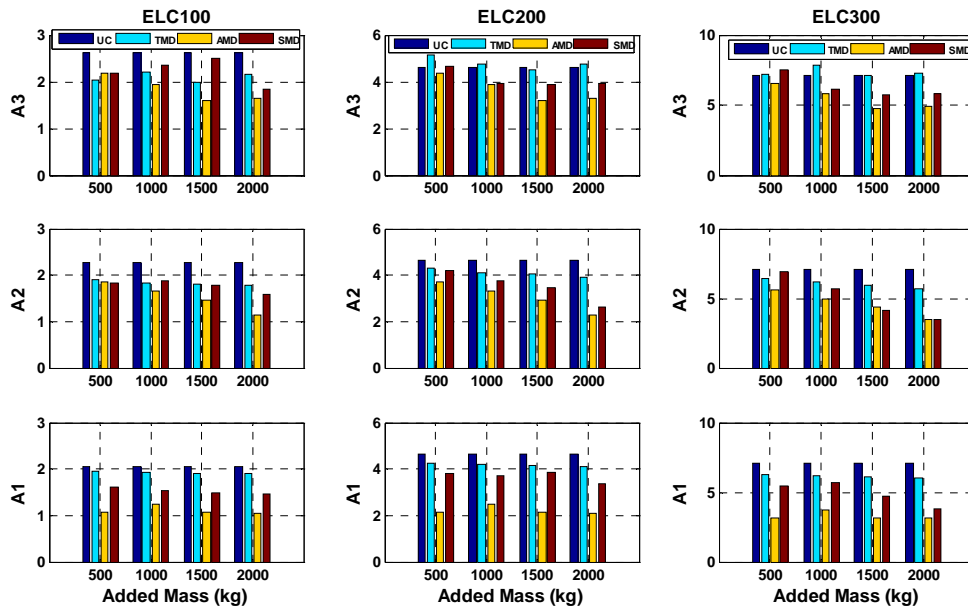


Fig. 7 Comparison of the maximum acceleration responses of uncontrolled structure, structure with passive TMD and semi-active SMD with different added mass, under El Centro earthquakes (normalized to 100, 200 and 300 gals)

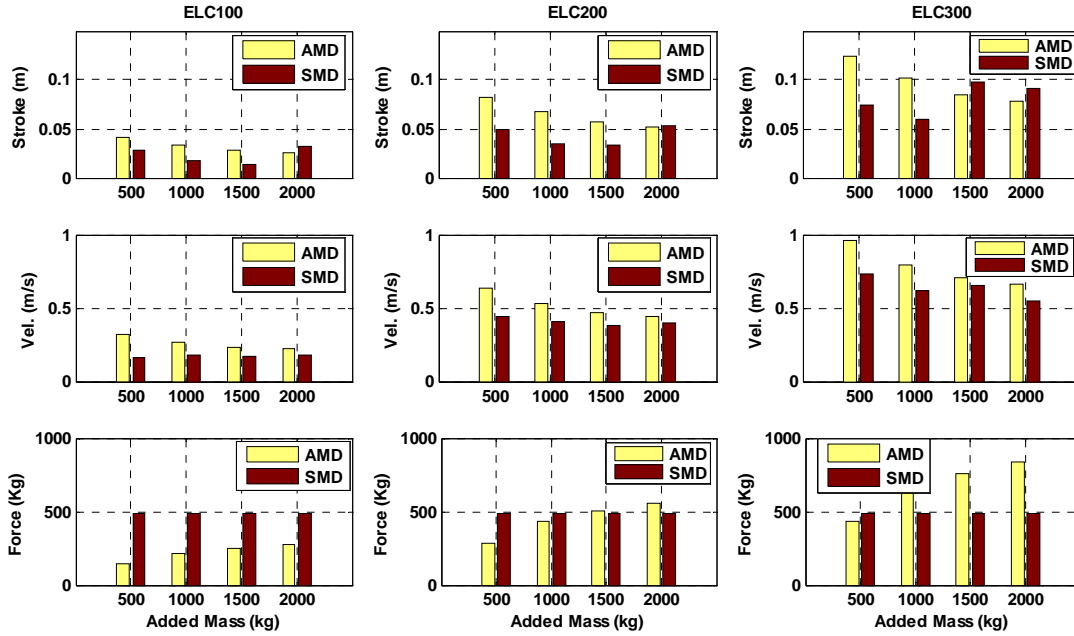


Fig. 8 Comparison of the maximum actuator/damper stroke, velocity and force of AMD and SMD with different added mass, under El Centro earthquakes (normalized to 100, 200 and 300gals)

although better performance can be implemented by the AMD, however, the large stroke, damper velocity and control force all show the difficulty of applying the AMD system in practice.

5. Experimental verification of the SMD system

The feasibility of implementing the proposed system in practice was verified through a shaking table test conducted at NCREE. A full-size three-story steel structure with each story measuring 3 m (length) × 2 m (width) × 3 m (height) and with the MR damper on the roof was used to form the four degree-of-freedom model in the theoretical analysis. In order to approach the assumption of a shear-type structure, the beams and the columns of the specimen were constructed using H-beams measuring 150 (mm) × 150 (mm) × 7 (mm) × 10 (mm) while the floor thickness was 25mm and was welded onto extremely strong floor plates. Additional blocks with a mass of 3.5 metric tons were mounted on every floor to satisfy the requirement of fundamental frequency. To demonstrate the practical performance of the SMD system under different mass ratios, the mass of the proposed system controlled by the MR damper on the roof measured 1 metric ton (5.5% of the total mass) and 2 metric tons (11.1% of total mass), respectively. The base of the system was mounted to the floor providing the remainder of the 6 metric tons of mass on the third floor. The case of added mass 500 kg was not conducted in the experiment since the mass block is relatively small compared to the weight of the 7 kN MR damper used in the experiment. The failure mode of the MR damper simulating the condition of MR damper with no power supply (SMD^F) was used



Fig. 9 Set-up of the three-story benchmark structure

to evaluate the robustness of the control system. The set-up including the specimen, the MR damper and the RPS, is shown in Fig. 9.

A traditional instrumentation system was deployed for the specimen to measure the response of the structure during earthquake excitation. As shown in Fig. 9, the absolute displacement, velocity and acceleration of each floor of the main structure as well as the reaction of the MR damper were recorded by linear variable differential transformer (LVDT) for comparison. The stroke of the MR damper was carefully monitored to avoid any collision between the MR damper and the specimen. The optimal control voltage was calculated by the embedded Simulink/dSPACE code (dSPACE 2005) with the necessary feedback signals and then sent to the MR damper. The control flow-chart of the proposed SMD system is shown in Fig. 10.

Four diverse earthquakes including the 1940 El Centro earthquake (NS direction), the 1995 Kobe earthquake, the TCU068 site record, and the TCU129 site record of the 1999 Chi-Chi earthquake, representing typical far-field and near-fault earthquakes were used to examine the practical performance of the SMD system. For each test case, the PGA value started from 50 gal with increments of 50 gal until the maximal allowable stroke of the MR damper, set at 12 cm in the experiment, was reached. To demonstrate the advantage of applying the proposed system, two different mass ratios of the SMD system were considered and five control modes, UC, SMD^F-1t, SMD^F-2t, SMD-1t and SMD-2t were executed where SMD^F represents the failure-mode of the SMD system with no power supplied on the MR damper. As mentioned in the theoretical analysis section, due to the high velocity and stroke which are hard to implement in practice, the AMD

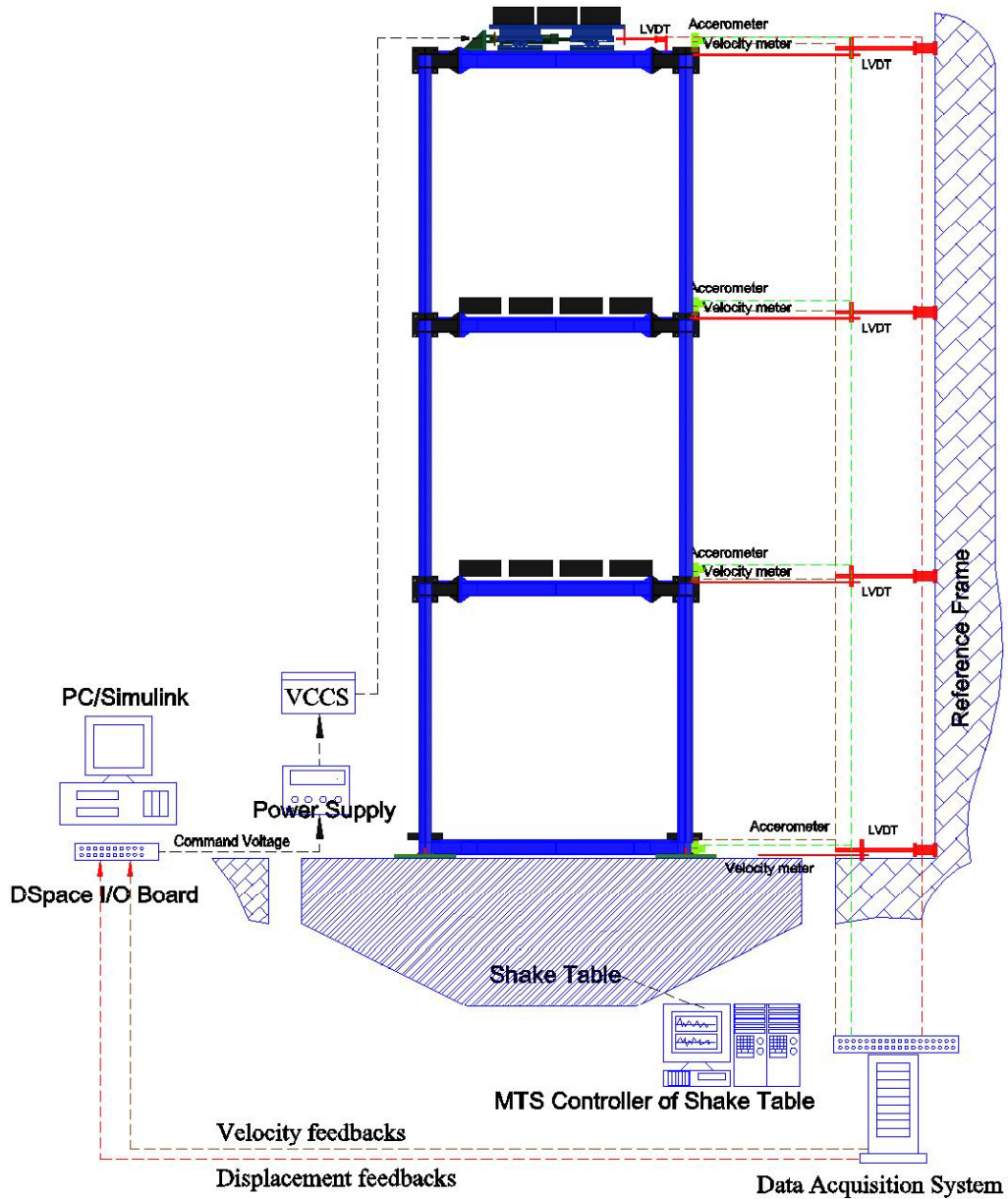


Fig. 10 Control flow-chart of the SMD damping system

system was not considered during the experiment. The experimental data were collected by the data acquisition system for further comparison.

Experimental results of specific cases are shown in Tables 4 and 5 where the absolute acceleration (A_1 , A_2 and A_3) and relative displacement of each floor (D_1 , D_2 and D_3) of the main structure are listed complete with the response of the MR damper (A_D , D_D and F_D). For the 1940 El Centro earthquake, three cases with different PGA value (100 gal, 200 gal and 300 gal) were carefully investigated. In the case of the PGA value of 100 gal, representing the level of a small

earthquake, the relative displacement of the roof was suppressed by each of the 2 SMD systems from 3.9 cm to 2 cm (SMD-2t) and to 2.25 cm (SMD-1t) while an approximate value of 2.1 cm and 2.44 cm were obtained by the SMD^F-2t and SMD^F-1t modes. The roof acceleration was reduced from 2.6311 m/s² to 1.84 m/s² for the SMD-2t mode while only minor improvements to 2.22 m/s², 2.2564 m/s² and 2.2281 m/s² were achieved by the SMD-1t, SMD^F-2t and SMD^F-1t modes, respectively. The structural response investigated was not seriously affected by the different mass ratios or the control methods including the SMD and SMD^F at this stage.

However, the results from the SMD systems were more successful in the case of the PGA value of 200 gal, which indicates a level of a moderate earthquake. The response of the main structure in four different modes are shown in Table 4. As indicated, the relative displacement of the second floor was alleviated from 7.08 cm to 3.28 cm, a reduction of 53.67 % for the SMD-2t case. The performance of SMD-1t was slightly degraded by its inherent mass ratio, but the displacement of 4.04 cm (42.9 %) was still better than the cases of SMD^F-1t (4.17cm) and SMD^F-2t (4.31 cm). The absolute acceleration of the second floor was mitigated from 4.68 m/s² to about 3.00 m/s² for all four control cases.

An interesting phenomenon could be investigated for the case of a PGA value of 300 gal, expressing a destructive major earthquake. The relative displacement of the third floor was successfully mitigated to 6.92 cm (SMD-2t) and 8.3 cm (SMD-1t) when a larger 9.46 cm response occurred with only 181 gal PGA for the uncontrolled case. Moreover, the absolute acceleration of the third floor was kept at a similar level, 7.13 m/s² and 7.03 m/s² compared to the uncontrolled

Table 4 Experimental result of the El Centro earthquake with different PGA values

El Centro										
	PGA (m/s ²)	A ₁	A ₂	A ₃	D ₁ (m)	D ₂	D ₃	A _D	D _D	F _D (KN)
UC	0.9118	1.8429	2.0312	2.6311	0.0153	0.0283	0.039			
	1.8145	4.3044	4.6806	6.4532	0.0369	0.0708	0.0946			
SMD ^F 1t	0.9859	1.4557	1.6207	2.4690	0.0111	0.0205	0.0244	0.7225	0.0349	0.2441
	1.8122	3.0967	3.1993	4.7158	0.0229	0.0417	0.0494	1.4678	0.0772	0.5667
SMD ^F 2t	0.9344	1.3169	1.1657	2.2564	0.0093	0.0162	0.021	0.9909	0.037	1.8009
	1.9317	3.1104	2.9917	5.0973	0.0232	0.0431	0.0519	1.4596	0.0761	2.5222
SMD 1t	0.9669	1.2996	1.4339	2.2281	0.0105	0.0192	0.0225	2.7916	0.0211	6.4900
	1.9269	2.7110	3.0818	4.3484	0.0225	0.0404	0.0481	4.2206	0.0410	6.0850
	2.7825	4.4813	4.9109	7.0389	0.0365	0.0667	0.083	5.0537	0.0846	7.3987
SMD 2t	0.973	1.5089	1.4322	1.8403	0.0097	0.0174	0.02	2.3073	0.0362	4.8153
	2.0962	2.5854	3.0919	5.0792	0.0194	0.0328	0.0443	2.8771	0.0668	5.8428
	2.9202	4.144	4.3528	7.1329	0.0299	0.0538	0.0692	3.2715	0.1125	6.2835

case of 6.45m/s^2 under PGA value 181 gal. Due to the 10 cm limited stroke of the MR damper during the experiment, only the SMD-1t and the SMD-2t nodes were executed in this stage since the stroke of the SMD^F systems had reached more than 7 cm under the El Centro 200 gal experiment. This result demonstrated that the SMD systems can adaptively change its control objective during different intensities of earthquake.

The overall presentation of the two SMD modes under different PGA levels of the El Centro earthquake, representing a regular far-field earthquake, is illustrated in Fig. 11. The blue line representing the performance of the SMD-2t method occupies the lowest position for almost every PGA value. This trend proves that the MR damper can perform well by using the proposed control algorithm with only adding 5.5% mass on the top, which is feasible in practice. Moreover, approximately 20 % efficiency increase over the SMD-1t system can be achieved if 11% mass is implemented.

The time histories of the roof response in the longitudinal direction with the two SMD systems under the El Centro earthquake with a PGA value of 200 gal are shown in Fig. 12. The trend shows that a slight improvement can be found in the displacement time history for the SMD-2t system,

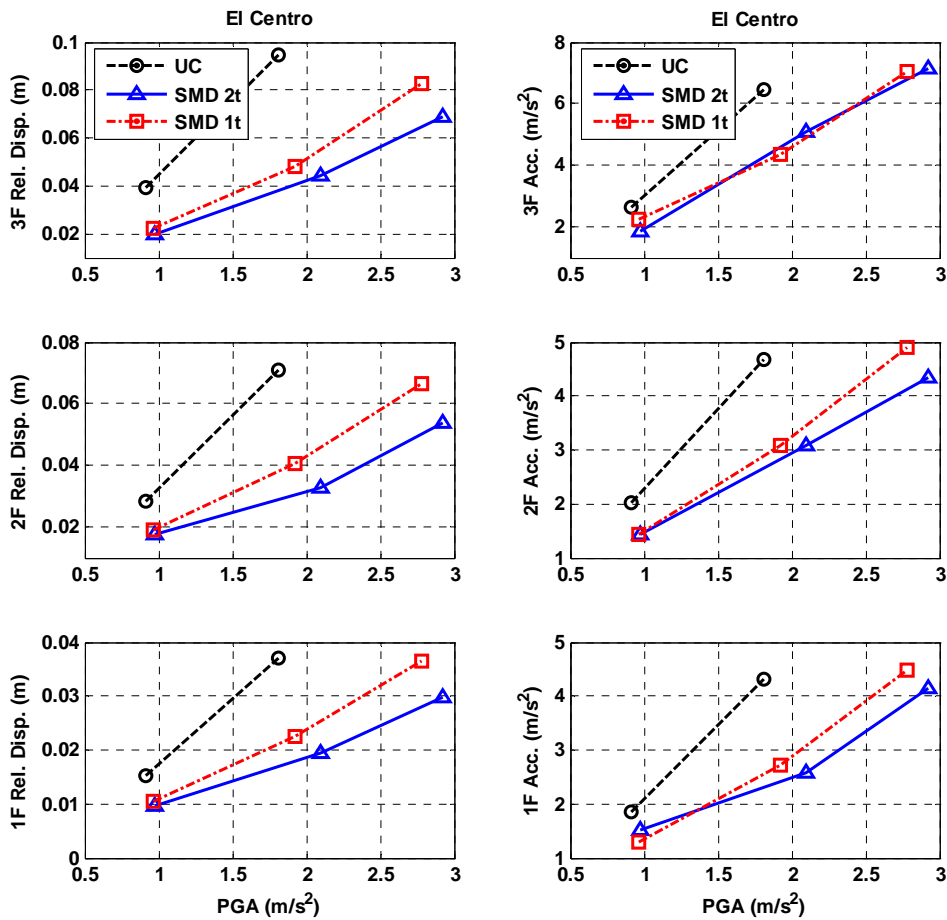


Fig. 11 Overall presentation of all modes under different PGA levels of the El Centro earthquake

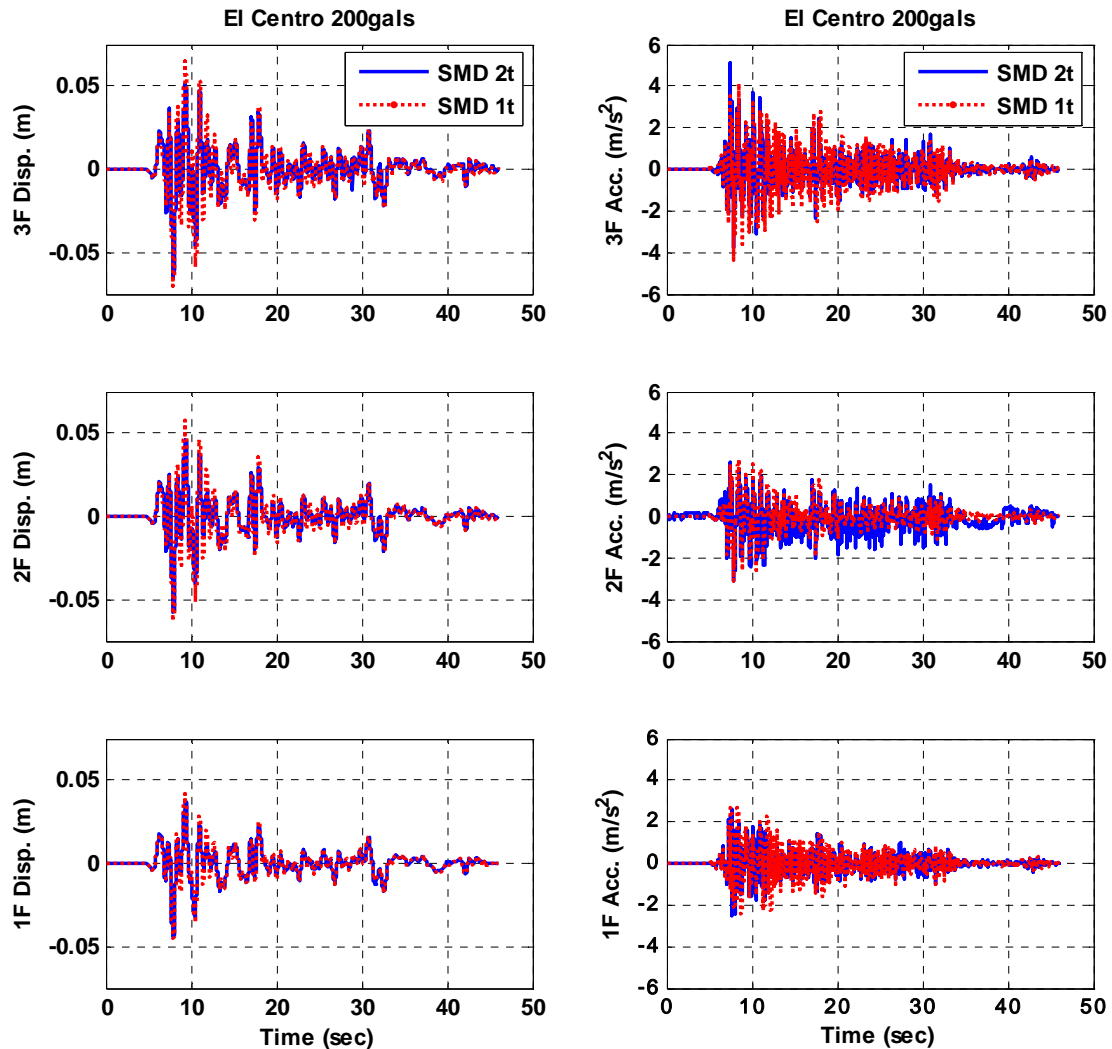


Fig. 12 Time histories of the main structure under the El Centro earthquake with a PGA value of 200gal

and that the acceleration responses under different mass ratios almost coincide with each other.

The results of the PGA value of 150 gal under the Kobe earthquake, and the PGA value of 200 gal for the TCU068 site record of the Chi-Chi earthquake are shown in Table 5 to demonstrate the ability of the SMD system when facing diverse earthquake characteristics. For the case of the Kobe earthquake, satisfactory displacement and acceleration reductions were recorded. Compared to the SMD^F-1t and SMD^F-2t modes, the roof movement was modified from 9.78 cm to 4.07 cm showing a dramatic improvement of 58.3 % while the acceleration was also ameliorated from 4.8383 m/s^2 to 3.0326 m/s^2 in the $SMD-2t$ case. Although the PGA value of $SMD-1t$ reached 182 gal during the experiment, the structural response was still controlled within an acceptable range. A clearer demonstration of all modes under different PGA levels of the Kobe earthquake is shown in Fig. 13.

In addition, the SMD systems also performed well under the excitation of the TCU068 time

Table 5 Experimental results of the Kobe and the Chi-Chi earthquake with different PGA values

Kobe										
PGA (m/s ²)	A_1	A_2	A_3	D_1 (m)	D_2	D_3	A_D	D_D	F_D (KN)	
UC	1.3976	2.5153	3.5704	4.8383	0.039	0.0774	0.0978			
SMD ^F 1t	1.3107	2.5186	3.6428	4.4011	0.0318	0.0592	0.0706	1.7767	0.0931	0.7253
SMD ^F 2t	1.4409	2.6348	3.7157	4.3185	0.0335	0.0643	0.0767	1.3508	0.0888	2.3795
SMD 1t	1.8269	3.4808	5.8243	6.6090	0.0434	0.0826	0.0966	5.8525	0.1143	6.1074
SMD 2t	1.7824	2.2796	4.9505	3.7597	0.0295	0.0570	0.0682	3.2367	0.0986	6.7814

ChiChi/TCU068										
PGA (m/s ²)	A_1	A_2	A_3	D_1 (m)	D_2	D_3	A_D	D_D	F_D (KN)	
UC	2.023	3.465	2.8884	4.9755	0.0267	0.0501	0.0696			
SMD ^F 1t	1.4180	2.2261	1.8377	3.1331	0.0169	0.0297	0.0361	1.2191	0.1032	0.4512
SMD ^F 2t	1.5124	2.2579	1.5557	2.9215	0.0163	0.0286	0.0358	0.8244	0.0874	0.9872
SMD 1t	1.9185	2.1992	2.4700	3.0252	0.0220	0.0390	0.0480	4.5097	0.0769	6.8673
SMD 2t	2.0877	1.8784	3.2496	3.5238	0.0208	0.0387	0.0483	3.3345	0.1098	5.9097

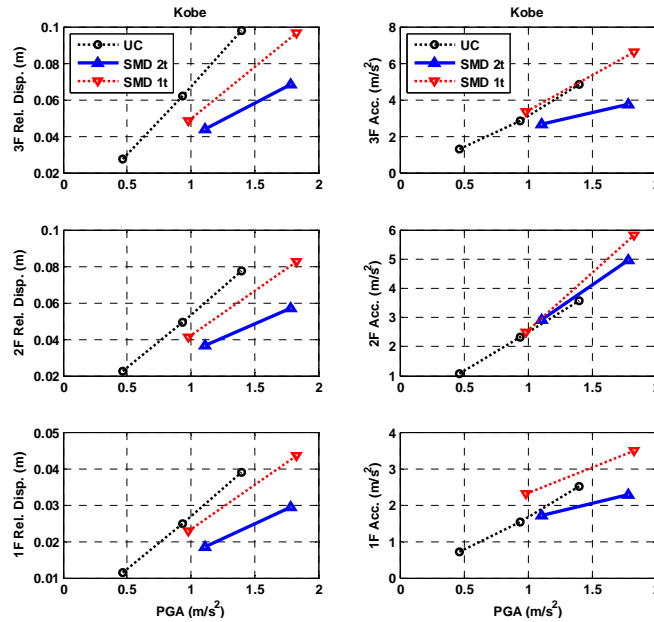


Fig. 13 Overall presentation of all modes under different PGA levels of the Kobe earthquake

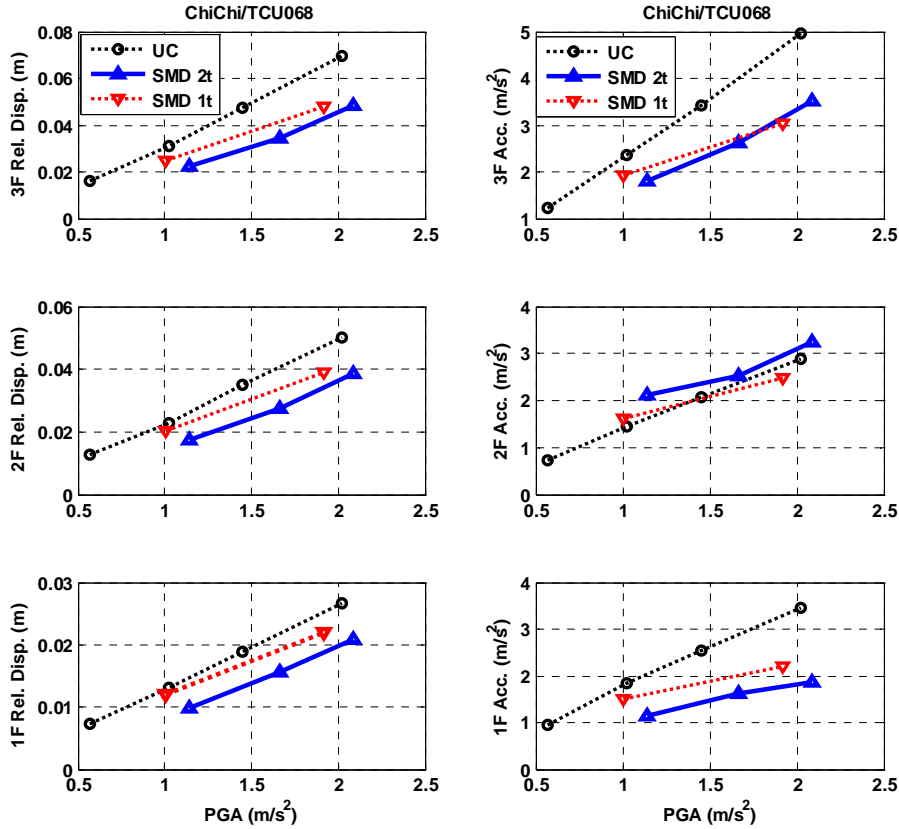


Fig. 14 Overall presentation of all modes under different PGA levels of the ChiChi/TCU068 earthquake

history of the Chi-Chi earthquake, a typical near-fault earthquake record which is generally difficult to deal with. With the help of the SMD system, the stroke, D_D , can be effectively controlled under the limitation of 10 cm, and the structure can be tested under PGA value 200 gal to verify their performance with the uncontrolled condition when the stroke of the SMD^F cases rapidly exceeded the 10 cm limitation in the level of PGA value 150 gal. The roof displacement, D_3 , was improved from 6.93 cm of the controlled case to 4.8 cm and 4.83 cm of SMD-1t and SMD-2t, respectively. Moreover, the roof acceleration, A_3 , was also successfully reduced from 497.5 gal to 302.52 gal and 352.387 gal. A mitigation rate of approximately 30% was observed both in relative displacement and absolute acceleration by applying the SMD-1t and SMD-2t control systems. The peak responses of all modes under different PGA levels of the ChiChi/TCU068 earthquake are illustrated in Fig. 14.

In summary, for the typical near-fault earthquakes such as the Kobe and TCU068 records, only slight differences were observed between different mass ratios, as shown in Table 5, and on average 30-40% displacement reduction and 40% acceleration reduction can be expected when using a 5.5 % mass ratio setting. Meanwhile, the displacement control efficiency under far-field earthquakes with wider frequency contents can be improved by up to 50- 60 % by increasing the mass ratio from 5.5 % to 11 %, and a similar acceleration reduction performance is obtained. For that reason, the 5.5% mass ratio (STM-1t) may be the most feasible choice in practice.

7. Conclusions

A novel SMD system using MR dampers is proposed in this research. To integrate the robustness of the traditional TMD system and the excellent control performance of the AMD system, the frictionless RPS and the MR damper are used to construct the proposed system using a full-scale three-story building as the benchmark structure.

To accurately predict the behavior of the designated large-stroke MR damper, a new approach combining seven numerical models and the interpolation technique was proposed. Seven sets of parameters describing the relationship between the velocity and the damping force under fixed voltages were used to form the database, and the damping force with arbitrary velocity and voltage was then calculated by the interpolated coefficients. The MR damper model was verified by the performance test at NCREE. The result has shown that both the time history and the hysteresis loop of the MR damper can be estimated correctly by the numerical model.

A new control algorithm with the continuous–optimal control concept was developed considering the success of the proposed numerical MR damper model. To provide an objective control outcome, all floor responses including relative displacement, relative velocity and absolute acceleration of the benchmark structure were considered in the performance index of the control algorithm. The command voltage was then calculated by the continuous–optimal control concept by interpolation between the best two voltage levels. The proposed SMD theory was verified by several typical earthquakes with different mass ratios. The numerical simulation demonstrated that the structural response can be satisfactorily alleviated by the SMD system.

The practical performance of the SMD system was carried out by a series of shaking table tests at NCREE for diverse earthquakes. The experimental results has proven that the MR damper can be manipulated properly by the proposed control algorithm with on average improvement in displacement of 30-40% and an improvement of 40 % in acceleration over the uncontrolled state under both far-field and near-fault earthquakes when a 5.5 % mass ratio is installed on the top of the structure. Moreover, the displacement control efficiency can be improved to approximately 50-60% by using an 11 % mass ratio for a far-field earthquake with a comparable acceleration reduction performance. In addition, compared to the alternative solution of deploying dense seismic dampers throughout the structure, the proposed SMD system on the roof can be much easier implemented and with a similar reduction percentage. The result of this study greatly support the practicability of the proposed system.

This study proposed a new SMD system including such techniques as a numerical approach of MR damper, the interpolation process, and the continuous–optimal control concept to enhance the practicability and reliability of the SMD system. The theoretical results and the experimental verification all demonstrate that the new system can successfully mitigate the response of the main structure in low- and mid-rise buildings by slightly increasing the strict restriction of mass ratio in high-rise buildings. The proposed SMD system can be easily implemented in practice.

References

- Bakre, S.V. and Jangid, R.S. (2007), “Optimum parameters of tuned mass damper for damped main system”, *Struct. Control Health M.*, **14**(3), 448-470.
- Brock, J.E. (1946), “A note on the damped vibration absorber”, *J. Appl. Mech.-ASME*, **64**(4), A-284.
- Chang, C.C. and Henry, T.Y. Yang (1995), “Control of buildings using active tuned mass dampers”, *J. Eng.*

- Mech.*, **121**(3), 355-366.
- Den Hartog, J.P. (1947), *Mechanical vibrations* (3rd edn), McGraw-Hill, New York.
- dSPACE Release 4.2 (2005), *Solution for control*, dSPACE GmBH, Germany
- Frahm, H. (1911), *Device for damping of bodies*, U.S. Patent No. 989, 958.
- Gregory, J. and Wereley, Norman M. (2000), "Seismic response of civil structures utilizing semi-active MR and ER bracing systems Hiemenz", *J. Intel. Mat. Syst. Str.*, **10**(8), 646-651.
- Kim, H.S., Roschke, P.N., Lin, P.Y. and Loh, C.H. (2006), "Neuro-fuzzy model of hybrid semi-active base isolation system with FPS bearing and MR damper", *Eng. Struct.*, **28**(7), 947-958.
- Lee, S.H., Min, K.W., Chung, L., Lee, S.K., Lee, M.K., Hwang, J.S., Choi, S.B. and Lee, H.G. (2007), "Bracing systems for installation of MR dampers in a building structure", *J. Intel. Mat. Syst. Str.*, **18**(11), 1111-1120.
- Loh, C.H. and Chern, W.Y. (1994), "Seismic effectiveness of active tuned mass dampers for the control of flexible structures", *Probab. Eng. Mech.*, **9**(4), 225-234.
- Mackriell, L.E., Kwok, K.C.S. and Samali, B. (1997), "Critical mode control of a wind-loaded tall building using an active tuned mass damper", *Eng. Struct.*, **19**(10), 834-842.
- MATLAB, User's Guide (1992), *The MathWorks, Inc.*: Natick, MA 01760.
- Nishitani, A. and Inoue, Y. (2001), "Overview of the application of active/semiactive control to building structures in Japan", *Earthq. Eng. Struct. D.*, **30**(11), 1565-1574.
- Ormondroyd, J. and Den Hartog, J.P. (1928), "The theory of the dynamic vibration absorber", *Trans.-ASME*, APM-50-7, 9-22.
- Pinkaew, T. and Fujino, Y. (2001), "Effectiveness of semi-active tuned mass dampers under harmonic excitation", *Eng. Struct.*, **23**(7), 850-856.
- Qu, Z.Q., Shi, Y. and Hua, H. (2001), "A reduced-order modeling technique for tall buildings with active tuned mass damper", *Earthq. Eng. Struct. D.*, **30**(3), 360-362.
- Rabinow, J. (1948), "The magnetic fluid clutch", *AIEE Trans.*, **67**(2), 1308-1315.
- Renzi, E. and Serino, G. (2004), "Testing and modelling a semi-actively controlled steel frame structure equipped with MR dampers", *Struct. Control Health M.*, **11**(3), 189-221.
- Ricciardelli, F., Occhiuzzi, A. and Clemente, P. (2000), "Semi-active tuned mass damper control strategy for wind-excited structures", *J. Wind Eng. Ind. Aerod.*, **88**(1), 57-74.
- Rudinger, F. (2007), "Tuned mass damper with nonlinear viscous damping", *J. Sound Vib.*, **300**(3-5), 932-948.
- Sakamoto, M., Kobori, T., Yamada, T. and Takahashi, M. (1996), "Practical applications of active and hybrid response control systems and their verifications by earthquake and strong wind observations", *Proceedings of First World Conference on Structural Control*, Los Angeles, CA, USA.
- Setareh, M. (2001), "Use of semi-active tuned mass dampers for vibration control of force-excited structures", *Struct. Eng. Mech.*, **11**(4), 341-356.
- Shook, D., Lin, P.Y., Lin, T.K. and Roschke, P.N. (2007), "A comparative study in the semi-active control of isolated structures", *Smart Mater. Struct.*, **16**(4), 1433-1446.
- Spencer, B.F., Dyke, S.J., Sain, M.K. and Carlson, J.D. (1997), "Phenomenological model for magnetorheological dampers", *J. Eng. Mech.*, **123**(3), 230-252.
- Yamamoto, M., Aizawa, S., Higashino, M. and Toyama, K. (2001), "Practical applications of active mass dampers with hydraulic actuator", *Earthq. Eng. Struct. D.*, **30**(11), 1697-1717.
- Yang, J.N., Bobrow, J., Jabbari, F., Leavitt, J., Cheng, C.P. and Lin, P.Y. (2007), "Full-scale experimental verification of resettable semi-active stiffness dampers", *Earthq. Eng. Struct. D.*, **36**(9), 1255-1273.
- Yang, R., Zhou, X. and Liu, X. (2002), "Seismic structural control using semi-active tuned mass dampers", *Earthq. Eng. Eng. Vib.*, **1**(1), 111-118.
- Zuo, L. and Nayfeh, S.A. (2005), "Optimization of the individual stiffness and damping parameters in multiple-tuned-mass-damper systems", *J. Vib. Acoust.*, **127**(1), 77-83.